Interaction of amino acid-functionalized silver nanoparticles and Candida albicans polymorphs: A deep-UV fluorescence imaging study

Radovan V Dojčilović, Jelena G Pajović, Dušan G Božanić, Una V Bogdanovic, Vesna V Vodnik, Suzana K Dimitrijević-Branković, Miona G Miljkovic, Slavka G Kaščaková, Matthieu M. Refregiers, Vladimir V Djoković

Interaction of amino acid-functionalized silver nanoparticles and *Candida albicans* polymorphs: a deep UV fluorescence imaging study

Radovan Dojčilović[1], Jelena D. Pajović[2,3], Dušan K. Božanić[1,4*], Una Bogdanovic[1], Vesna V. Vodnik[1], Suzana Dimitrijević-Branković[5], Miona G. Miljkovic[5], Slavka Kaščaková[3,6,7], Matthieu Réfrégiers[4] and Vladimir Djoković[1,*]

[1]*Vinča Institute of Nuclear Sciences, University of Belgrade, P.O. Box 522, 11001 Belgrade, Serbia*

[2]*Faculty of Physics, University of Belgrade, P. O. Box 368, 11001 Belgrade, Serbia*

[3]*DISCO beamline, Synchrotron SOLEIL, F-91192 Gif sur Yvette, France*

[4]*DESIRS beamline, Synchrotron SOLEIL, F-91192 Gif sur Yvette, France*

[5]*Department of Bioengineering and Biotechnology, Faculty of Technology & Metallurgy, University of Belgrade, Karnegija 4, 11120 Belgrade, Serbia*

[6]*Inserm Unité 1193, F-94800 Villejuif, France*

[7]*Univ. Paris-Sud XI, UMR-S1193, F-94800 Villejuif, France*

Abstract

The interaction of the tryptophan functionalized Ag nanoparticles and live *Candida albicans* cells was studied by using synchrotron excitation deep-ultraviolet (DUV) fluorescence imaging at the DISCO beamline of Synchrotron SOLEIL. DUV imaging showed that incubation of the fungus with functionalized nanoparticles results in significant increase in the fluorescence signal. The analysis of the images revealed that the interaction of the nanoparticles with (pseudo)hyphae polymorphs of the diploid fungus was less pronounced than in the case of yeast cells or budding spores. The changes in the intensity of the fluorescence signals of the cells after incubation were followed in [327 - 353 nm] and [370 – 410 nm] spectral ranges, which correspond to the fluorescence of tryptophan in non-polar and polar environment, respectively. As a consequence of the environmental sensitivity of the silver-tryptophan fluorescent nanoprobe, we were able to determine the possible accumulation sites of the nanoparticles. The analysis of the intensity decay kinetics showed that the photobleaching effects were more pronounced in the case of the functionalized nanoparticle treated cells. The results of time-integrated emission in the mentioned spectral ranges suggested that the nanoparticles penetrate the cells, but that the majority of the nanoparticles were situated on the cells' surfaces.

Keywords: silver nanoparticles, tryptophan, functionalization, *C. albicans*, fluorescence imaging

*Corresponding authors: bozanic@vinca.rs; djokovic@vin.bg.ac.rs

Introduction

Candida albicans is a polymorphic fungus and a common pathogen that threatens the immunosuppressed patients. The most pronounced infectious effect of *C. albicans* is an adhesion to the host cells, which is usually followed by agglomeration and biofilm formation. Transformation from yeast to hyphae is recognized as a therapeutic target in the *C. albicans* infections [1] and various approaches are suggested to suppress this particular morphological transition [2-4]. One of the suggested approaches includes using silver nanoparticles (Ag NPs), either alone or in combination with other drugs, in treatment of pathogenic fungi [5-16]. For example, Lara et al. [8] reported that silver nanoparticles might induce inhibition in filamentation growth of pre-formed *C. albicans* biofilms. Kim et al. [9] provided detailed study on activity of Ag NPs against *C. albicans* cells, which mainly includes the disruption of cell membrane and inhibition of the budding process. It was also reported that the nanoparticles may arrest the fungal cell cycle in G2/M phase and stop the mitosis. Glucose and trehalose release was increased in the presence of Ag NPs, confirming their strong antifungal effect on the cell transport processes. The nano-silver induces intracellular accumulation of reactive oxygen species (ROS) and alters mitochondrial membrane potential [10]. Vazquez-Munoz et al. [11] used structural analysis to study the mechanism of interaction of Ag NPs with *C. albicans*. They reported that the nanoparticles tend to accumulate in the cell walls and induce cell death by releasing silver ions. Intermediate growth stages of biofilm formation are more vulnerable to the attack of antifungals [17]. The resistance of *C. albicans* to the action of silver nanoparticles gradually increases as their growth proceeded from adhered cells to pre-formed biofilm and, finally, to mature biofilm [13-14]. Therefore, in order to improve the antifungal treatments with nanoparticles, it is important to study and understand their interaction with the pathogen cells.

In our recent study [18], we reported on fabrication of a fluorescent probe sensitive to the polarity of the environment through functionalization of Ag NPs with amino acid tryptophan. The nanoprobe was tested on the cells of gram negative bacteria *Escherichia coli*. The deep UV fluorescence imaging of the *E. coli* cells incubated with tryptophan-functionalized Ag NPs (AgTrp NPs) showed that it is possible to distinguish whether nanoparticles were localized in hydrophobic (e.g. cell wall) or hydrophilic (cell interior and/or exterior) regions of the cells. Here, we also employed deep ultraviolet (DUV) fluorescence imaging method to investigate whether in this way created fluorescent probe may be used to provide information about the interaction of the silver nanoparticles and *C. albicans* at various morphogenetic stages of its growth. Comparing to the conventional imaging techniques, this method enables excitation of fluorophores at wavelengths below 300 nm, which may significantly increase the resolution of fluorescence images [19-21]. Tryptophan absorbs in the UV part of the EM spectrum and a high spatial resolution was achieved with AgTrp NPs fluorescence probe: one pixel ~150 nm [18]. For this reason, it was possible to detect the signal coming from the AgTrp nanostructures after their interaction with *C. albicans*. The fluorescence photobleaching in the [327 – 353 nm] and [370 - 410 nm] emission spectral ranges after the cell treatment was studied to establish the preferential nanoparticle accumulation sites.

Materials and methods

2.1. Materials

We used high purity water with specific resistance ~10^{18} Ωm in all synthetic procedures. Chemicals employed for making functionalized nanoparticles were silver nitrate ($AgNO_3$), sodium borohydride

($NaBH_4$), sodium hydroxide (NaOH) and tryptophan (Trp), which were purchased from Sigma-Aldrich and used as received.

2.2. Tryptophan functionalized silver nanoparticles

Silver hydrocolloids (Ag NP) and hydrocolloids of tryptophan-functionalized silver nanoparticles (AgTrp) were prepared in the same way as in our previous work [18]. Briefly, silver nanoparticles were prepared by chemical reduction of silver salt ($AgNO_3$) by using $NaBH_4$. Functionalization was carried out by adding appropriate amount of tryptophan to silver hydrocolloid with pH value adjusted to 10.4. List of samples used in this study is given in Table 1.

Table 1. Sample annotations, concentration, volume and molar ratio of chemicals used in the preparation procedure.

Sample	*V* (0.1 mM Ag NP) [ml]	*V* (10 mM Trp) [ml]	n_m (Ag): n_m (Trp)[b]
Trp2.0	0[a]	0.2	0
Ag NPs	10	0	∞
AgTrp1.0	10	0.1	1:1
AgTrp2.0	10	0.2	1:2

[a]in 10 ml H_2O; [b]Ag:Trp molar ratio.

The incubation of the *C. albicans* cells with functionalized nanoparticles was performed in the saline medium. Saline can induce the changes in the optical properties of silver nanoparticles. To test the stability of the nanoparticles, the hydrocolloids were mixed with 0.9% NaCl. The procedure was the same as the incubation procedure (explained below), but with no cells present.

In order to show the sensitivity of photoluminescence of tryptophan functionalized silver nanoparticles on the polarity of the environment, the phase transfer of AgTrp2.0 hydrocolloid from water to toluene was performed. The phase transfer was possible solely with functionalized nanoparticles, which was confirmed by mixing the toluene with Ag NPs hydrocolloid. Details about the procedure and images of the test tubes containing AgTrp NPs and Ag NPs in water and toluene can be found in Supporting information (Figure S1).

2.3. Preparation of biological samples

2.3.1 Strain, growth and media conditions

The growth of pathogen fungus *C. albicans* (ATCC 10259) strain was carried out in a Trypton Soy broth or agar (TSYB or TSYA—Institute of Immunology and Virology, Torlak, Belgrade), supplemented with 0.6% (v/v) yeast extract. For inoculum preparation, the microorganisms were cultivated in TSYB at 37 °C and left overnight (early exponential stage of growth). The culture media was prepared using distilled water and sterilized by conventional methods.

2.3.2 Antimicrobial activity and uptake tests

The solutions with specific concentrations of tryptophan, Ag NPs, and AgTrp NPs were prepared by mixing the colloids with sterile physiological saline solutions. After that, 400 µl of the solutions were placed in Eppendorf tubes containing 100 µl of purified microbial dispersion. The resulting mixture was vortexed for 10 s and incubated at 37 °C for two hours. In order to test the antimicrobial activity, the dispersions were placed in Petri dishes, overlaid with TSYA (0.6% of agar–agar in Trypton soy broth). After 24 h of incubation at 37 °C, the counts of viable microorganisms were determined. The results of antimicrobial activity are given in Supporting information (Figure S2).

Silver nanoparticles can inhibit yeast growth of *C. albicans* [16]. For this reason, we also conducted 24 h survival tests of *C. albicans* incubated with AgTrp2.0 in the presence of TSB as a growth medium. A delay in growth was observed during first 2 hours of incubation time (Supporting information, Figure S3). At higher incubation times (4, 8, 10 and 24 h), the growth trend is similar to that obtained for the control *C. albicans* sample.

The uptake test was performed after mixing of *C. albicans* dispersion with AgTrp2.0 colloid (the preparation procedure was the same as the one used for the antimicrobial tests). The mixture was centrifuged at 3000 rpm for 10 min. The optical densities at 400 nm were measured prior and after centrifugation of the mixture. For comparison, the OD400 values were also determined for the starting *C. albicans* dispersion (prior and after centrifugation) under the same conditions. The results of the uptake tests are presented in Supporting information (Table S1).

2.3.3 Preparation of biological samples for DUV imaging

The biological samples for DUV imaging were prepared by adding different volume ratios of tryptophan solution (Trp2.0) as well as Ag NPs and AgTrp2.0 colloids into 100 µl of purified *C. albicans* saline dispersions. The mixtures were incubated at 37 °C for 2 h and then 10 µl of each sample was placed on quartz coverslips. The samples were left to dry at ambient conditions. After that, they were washed with distilled water to remove unattached and dead cells and immediately examined by DUV fluorescence imaging. The control sample of untreated *C. albicans* cells was prepared by using the same procedures and conditions, but without adding the tryptophan solution and/or the colloids.

2.4. Methods

UV–vis absorption measurements were carried out by using Thermo Evolution 600 and Ultrospec 3300 spectrophotometer. Fluorescence spectra of the pure tryptophan solution and AgTrp colloids were recorded on a Perkin–Elmer LS45 fluorescence spectrophotometer.

DUV fluorescence imaging experiments were carried out at DISCO beamline of SOLEIL synchrotron facility, Saint Aubin, France. The fluorescence images of *C. albicans* cells and *C. albicans* cells incubated with tryptophan, Ag NPs, and AgTrp NPs were acquired on TELEMOS endstation of DISCO. Synchrotron UV radiation with wavelength of 290 nm was used as an excitation source and the luminescence signal was collected in the [327- 353 nm] and [370 - 410 nm] wavelength ranges for 30 seconds. To ensure consistency of the observations at least 10 different locations (155 x 60 µm) were investigated by means of DUV imaging. Ultrafluar glycerin immersion objective (Zeiss, Germany) with 100× magnification was used for collecting images. The fluorescence images were recorded by using PIXIS 1024-BUV EM-CCD camera (Princeton, USA). The whole setup was controlled by µManager [22] and the images were analysed by using FIJI software [23]. Step by step procedure for the processing of fluorescence images is explained in the Supporting information (Figure S4).

Bleaching kinetics was analysed by using a plugin PixBleach [24], developed in Fiji software. The intensities from the bleach stacks are fitted to Kohlrausch function, a generalized exponential function with an additional stretching parameter [25-27],

$$I(t)=A\times exp(-t/\tau)^{1/h}+B, \qquad \text{Eq. 1}$$

where *A* is the decay amplitude, *B* is a measure of the background autofluorescence, τ is the bleach time constant and *h* is the heterogeneity factor. Eq 1 was used to fit the fluorescence intensities of at least 10 images in a stack. The amplitude corresponded to initial fluorescence intensity (prior to bleaching). Bleach time constant is the parameter that characterizes the lifetime of the fluorophore in the structure, while heterogeneity factor is related to the width of the τ-distribution values. Time integrated emission (TIE) was estimated as the total signal intensity emitted by the fluorophores before their complete photodestruction. The stack images and calculated parameters are presented in detail in the results section.

Results and discussion

3.1. Optical properties of tryptophan-functionalized silver nanoparticles in water, saline and culture medium.

Figure 1a shows the UV-vis absorption spectra of the pure tryptophan water solution (Trp2.0) as well as Ag NPs, AgTrp1.0 and AgTrp2.0 hydrocolloids. In the case of the silver nanoparticle hydrocolloid, a typical absorption spectrum with pronounced surface plasmon resonance (SPR) band at ~398 nm was obtained. After the functionalization of Ag NPs with tryptophan, there is an asymmetric broadening and a slight shift of the SPR band, while the intensity of the band decreases. Also, an additional absorption band emerges at approximately 525 nm (Figure 1a). The obtained UV-vis spectra suggest that tryptophan induces agglomeration of the Ag NPs and this is discussed in detail in our previous study [18]. TEM analysis revealed that the functionalization induced an increase in diameter and a change in eccentricity of hybrid nanostructures formed [18].

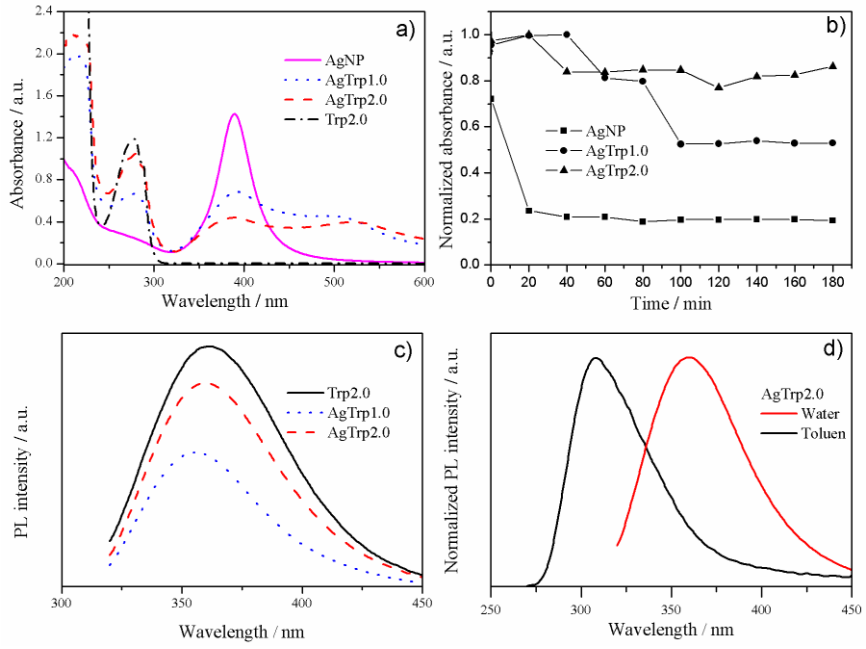

Figure 1. a) Absorption spectra of the pure tryptophan water solution (Trp2.0), silver hydrocolloids (Ag NPs) and hydrocolloids of tryptophan-functionalized silver nanoparticles (AgTrp1.0 and AgTrp2.0). b) The stability of Ag NPs and AgTrp1.0 and AgTrp2.0 colloids in saline solution. The stability was estimated by following the changes in the intensity of absorption at λ_{max} = 398 nm with time [28]. c) Photoluminescence emission (λ_{exc}=290 nm) spectra of tryptophan aqueous solution and AgTrp hydrocolloids. (d) Normalized photoluminescence spectra of AgTrp2.0 colloids in toluene (λ_{exc}=240 nm) and water (λ_{exc}=290 nm).

It was already mentioned in the experimental that a saline solution was used as a dispersion medium for *C. albicans*. Since the incubation was carried out in saline, it is important to test the chemical stability of tryptophan functionalized Ag NPs in this environment. Silver tends to form non-biocompatible complexes with chlorine and a decrease in the intensity of the SPR absorption band can be used as a measure of the stability of the nanoparticles [28]. Ag NPs, AgTrp1.0 and AgTrp2.0 hydrocolloids were mixed with saline at 37 $^{\circ}$C and the intensity of the absorbance at ~398 nm was monitored for 3 hours. The relative changes in the optical absorption of Ag NPs, AgTrp1.0 and AgTrp2.0 samples in saline with time were shown in Figure 1b. It can be seen that the bare silver nanoparticles (Ag NPs) are highly unstable in the presence of saline. The intensity of the absorption band at prolonged times dropped by almost 80%. Concerning the functionalized nanoparticles (AgTrp1.0 and AgTrp2.0), their concentration also decreases with time but to a lesser extent. In the case of the AgTrp2.0 sample the intensity of the SPR band was reduced by 10% only, meaning that the tryptophan prevents the complexation of silver with chlorine to a certain extent and, consequently, improves the stability of the nanoparticles in the saline solution.

The photoluminescence emission spectra of the pure tryptophan water solution (Trp2.0) and tryptophan functionalized silver nanoparticle hydrocolloids (AgTrp1.0 and AgTrp2.0) are presented in Figure 1c. An asymmetric emission band observed in the spectra of the three samples corresponds to the environmentally sensitive $^{1}L_{a}$ transitions of tryptophan. If AgTrp2.0 hydrocolloid is mixed with toluene, a phase transfer of the nanoparticles from polar to non-polar medium will occur, which is reflected in altered luminescence properties of the amino acid. The photoluminescence spectra of the initial and the phase transferred AgTrp2.0 colloids are given in Figure 1d. As it can be seen, a shift of the emission band towards lower wavelengths takes place after the transfer of the AgTrp2.0 nanoparticles into the non-polar environment.

Prior to fluorescence imaging, the optical density measurements at 400 nm (OD400) were used to test the uptake of AgTrp2.0 nanoparticles by *C. albicans* cells. First, OD400 was measured immediately after the mixing of AgTrp2.0 and *C. albicans*. After the mixing, it was found that the OD400 was reduced by about 30% with respect to the AgTrp2.0 in saline solution. *C. albicans* cells can contribute to this effect, so for this reason, the mixture was centrifuged and the optical density of the supernatant was measured. The obtained optical density of the supernatant was found to be half of the optical density of the initial AgTrp2.0 in saline. OD400 test performed on the supernatant of the control sample of the pure *C. albicans* cells showed virtually no attenuation of light at 400 nm. The results of the uptake test were included in the Supporting information (Table S1).

The present DUV imaging results concern the *C. albicans* incubated with AgTrp2.0 nanoparticles. As control samples for DUV imaging, we used untreated *C. albicans* cells and *C. albicans* cells mixed with pure tryptophan (Trp2.0) and bare silver nanoparticles Ag NPs.

3.2. Deep UV fluorescence imaging

The DUV fluorescence imaging studies of the pure *C. albicans* cells and *C. albicans* cells mixed with pure tryptophan solution (Trp2.0), Ag NPs colloid and AgTrp2.0 colloid were performed by using 290 nm synchrotron beam as an excitation source. The discussion of the results will be focused on the fluorescent signals obtained in [327 - 353 nm] (filter F1) and [370 - 410 nm] (filter F2) ranges. The signal collected in F1 range originates predominantly from the fluorescence of functionalized nanoparticles situated in non-polar environment, but a smaller part of the collected signal may also come from the fluorescence of the nanoparticles in water (low-wavelength tail in Figure 1). The signal

collected in F2 range belongs to the fluorescence of the functionalized nanoparticles situated in polar environment (water).

Prior to the discussion on the fluorescence imaging results, we will refer to the observations regarding the morphology of the untreated *C. albicans* and *C. albicans* after the incubation. The bright field imaging of the untreated *C. albicans* sample showed the presence of diverse morphogenetic states of the fungus: single cells, small clusters of yeast cells, budding yeast forms and larger clusters of agglomerated yeast as well as pseudohyphae and hyphae, whereas the later forms were not found in the *C. albicans* samples incubated either with pure tryptophan or Ag NPs. We have correlated this observation with the antimicrobial activity tests, which showed that the number of *C. albicans* colonies in the samples with tryptophan and Ag NPs were significantly reduced (Supporting information Figure S2). Since no mature morphogenetic forms were found in the above mentioned control samples, we compared the fluorescence signals arising from single yeast cells and small clusters of single cells.

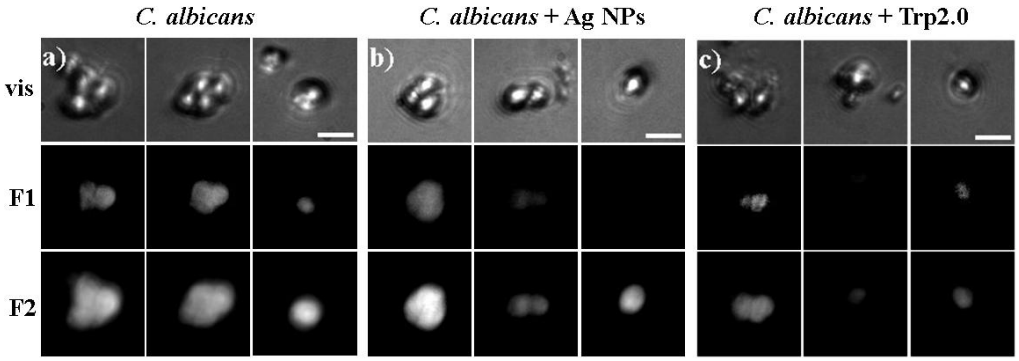

Figure 2. Bright field (vis) and fluorescence images of *C. albicans* single cells and small clusters of cells recorded in two emission ranges F1 [327 - 353 nm] and F2 [370 - 410 nm]: a) *C. albicans*, b) *C. albicans* incubated with bare Ag NPs and c) *C. albicans* incubated with Trp2.0. Scale bar is 5 μm. For comparison, the fluorescence signals in corresponding F1 and F2 channels were scaled to the same range of values using Fiji image analysis software.

Figure 2 shows the bright-field and the fluorescence images of the pure *C. albicans* cells and the cells incubated with tryptophan and bare Ag NPs. In order to be able to compare the fluorescence intensities, the fluorescence signals in the corresponding channels were scaled to the same range of values using Fiji image analysis software. The untreated cells (Figure 2a) exhibit autofluorescence in both spectral ranges, [327 - 353 nm] (filter F1) and [370 - 410 nm] (filter F2). The autofluorescence originates from the presence of the fluorophores in the cells such as phenylalanine, tryptophan and dityrosine [29,30]. Figure 2b and 2c show the fluorescence images of the cells after the incubation with tryptophan and Ag NPs. With respect to the intensity of the autofluorescence of the control sample, no significant changes in fluorescence were observed after the incubation. Statistical analysis was performed on the results obtained from at least 10 different locations along the sample and it confirmed that the variations in the intensity of the fluorescent signal were within the experimental error. Tryptophan and Ag NPs obviously affect the filamentation and growth [9,31], but do not affect the fluorescence properties of the cells.

In contrast to these observations, the pseudohyphae and large clusters of agglomerated yeast were observed in the case of *C. albicans* cells treated with the tryptophan functionalized silver nanoparticles. Although the antifungal activity of the AgTrp2.0 colloid was more pronounced than that of the pure tryptophan and bare silver nanoparticles (Supporting information, Figure S2), the similarity

between the growth curves of the sample and control (Supporting information, Figure S3) indicates that the treated cells reach the phase of stationary growth. This is probably the consequence of a lower diffusivity of functionalized nanoparticles, since they are larger in size than the starting Ag NP. In Figure 3, we show the fluorescent images of the pseudohyphae with budding spores in early stage of growth for the control *C. albicans* sample and the sample obtained after incubation of *C. albicans* with AgTrp2.0 nanoparticles (*C. albicans*+AgTrp2.0). It can be seen that the sample incubated with AgTrp2.0 nanostructures exhibits much stronger fluorescence than the control sample in both spectral ranges (F1 and F2). The intensity of the fluorescence signal increased almost three times proving that the tryptophan functionalized silver nanoparticles interacted with the cells. Specifically, there is a preferential interaction of AgTrp2.0 nanoparticles with the spores, rather than with the elongated parts of pseudohyphae. This result agrees with previous studies that showed that the morphogenetic forms in early stages of growth are less resistant to antifungal agents [8,17].

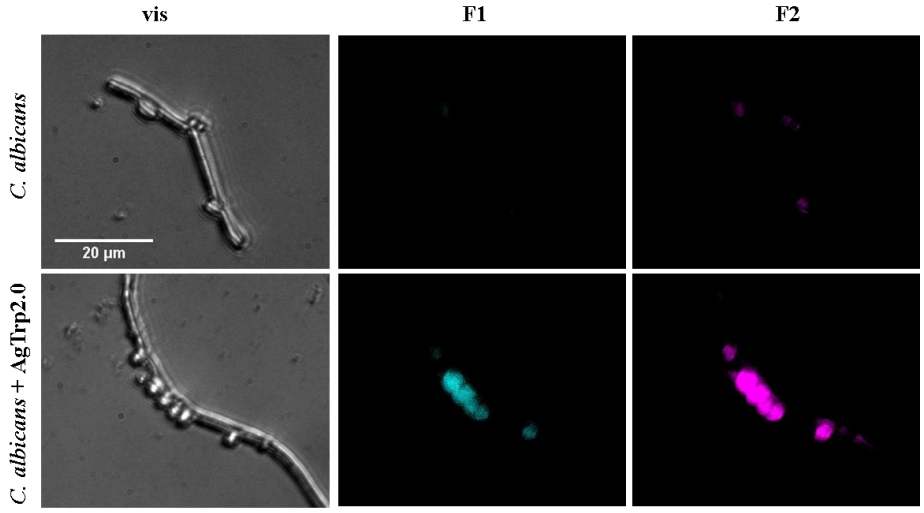

Figure 3. Bright-field (vis) and fluorescence images of pseudohyphae with budding spores in early stage of growth of the control *C. albicans* and *C. albicans*+AgTrp2.0 samples. The fluorescence images were obtained upon 290 nm synchrotron beam excitation, while the fluorescent signal was collected for 30 s in the [327 - 353 nm] (F1) and [370 – 410 nm] (F2) wavelength range. The fluorescence signals in corresponding F1 and F2 channels were scaled to the same range of values using Fiji image analysis software.

The fluorescence images in Figure 3 suggest that the incubation with AgTrp2.0 nanoparticles results in significant increase in fluorescence intensity in both spectral ranges (F1 and F2). In Figure 4, we show that this is also the case with the other morphogenetic forms of *C. albicans* such as the yeast and early biofilm phases. It can be seen in Figure 4a that the yeast and early biofilm forms incubated with AgTrp2.0 nanoparticles exhibit more pronounced fluorescence than that of the control sample (again, the fluorescence signals in corresponding F1 and F2 channels were scaled to the same range of values using Fiji image analysis software). In Figure 4d, we compare the mean fluorescence intensities per single cell calculated from at least ten different locations along the samples. It can be noticed that the mean florescence intensity in both spectral ranges increased by almost two times after the incubation. The obtained results clearly show that AgTrp2.0 nanoparticles affect the fluorescent properties of the *C. albicans* after the incubation. However, the fact that the fluorescence intensity increases in each of the investigated spectral ranges suggests that the functionalized silver nanoparticles may reside in both hydrophilic (cell interior and/or exterior) and hydrophobic (cell wall) regions of the cells.

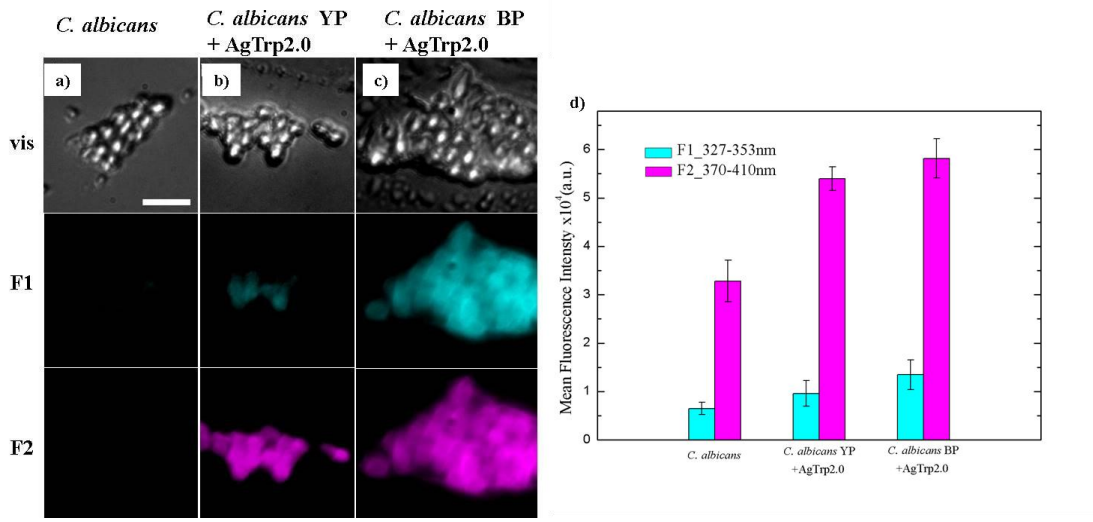

Figure 4. a) Bright-field and fluorescence images of a) control *C. albicans* cells b) AgTrp2.0 incubated *C. albicans* agglomerated yeast phase (YP) cells and c) AgTrp2.0 incubated *C. albicans* early biofilm phase (BP) cells. Scale bar is 10 μm. The fluorescence images were obtained upon 290 nm synchrotron beam excitation, while the fluorescent signal was collected for 30 s in the [327 - 353 nm] (F1) and [370 – 410 nm] (F2) wavelength ranges. d) Statistics on mean fluorescent intensity per single cell for untreated (control) and incubated (yeast phase and biofilm phase) *C. albicans* samples. The fluorescence signals in corresponding F1 and F2 channels were scaled to the same range of values using Fiji image analysis software.

The observed increase in the fluorescence signal intensity in both F1 and F2 spectral ranges in the *C. albicans* cells incubated with AgTrp2.0 nanoparticles in comparison to the control, opened up a possibility for drawing additional conclusions on the accumulation of the nanoparticles in the cells. To that end, we have performed time lapse experiments and bleach kinetics analysis of the results. In the image sequences obtained in the time lapse experiment, we selected 50 local maxima of fluorescence in the ranges to represent the specific sites at which accumulation of the nanoparticles takes place. To determine the fluorescence maxima, a threshold is set at the maximum value minus noise tolerance and the analyses were carried out over the contiguous area around the maximum which is above the threshold (the details of the procedure can be found in Supporting information). It was observed that the fluorescence intensity values of the local maxima were significantly higher than the autofluorescence of the control sample. This approach was used instead of co-localisation analysis due to heterogenic nature of *C. albicans* autofluorescence as well as due to the problems in establishing well-defined crosstalk parameters.

Figure 5 shows the dependence of the local fluorescence maxima values on time (the box plot diagrams) for the untreated and treated cells that constitute early biofilm phase. In the case of the control sample, the autofluorescence is decreasing with time in both spectral ranges (Figure 5a). The same is observed for the incubated cells (Figure 5b) but with more pronounced decay of the intensity of fluorescence signal over the same period. Taking also into account that incubated cells show overall higher intensity of fluorescence signals, the results in Figure 5 suggests that they contain the fluorophores that exhibit different bleaching kinetics. To elucidate this effect further, we decided to study in detail the changes in the fluorescence intensity in both emission channels during the bleaching by analysing the consecutive fluorescence images of the cells. In the mentioned analyses, the stretched exponential decay function (Eq. 1) was used. The calculations are based on pixel by pixel analysis of the randomly distributed bleach rate constants, which is appropriate for heterogeneous fluorescence coming from robust structure such as early biofilm [26,27].

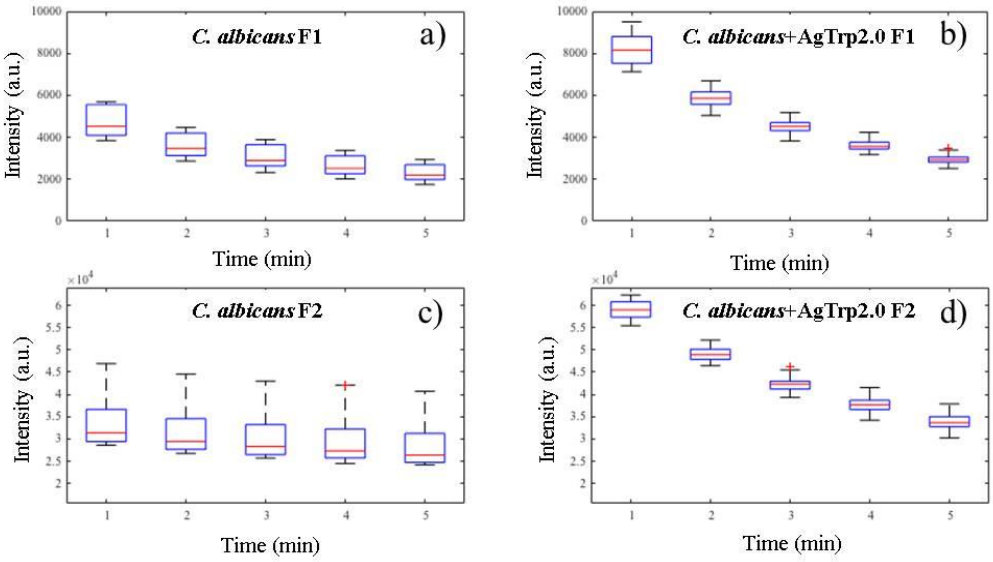

Figure 5. The box plot diagrams of the local fluorescence maxima values *versus* time for untreated (a, c) and incubated (b, d) cells in [327 - 353 nm] (F1) and [370 – 410 nm] (F2) spectral ranges. Red horizontal line represents the median intensity of the corresponding maxima (see Figure S4 in supporting information for details).

Five selected images from the time lapse stack are presented in Figure 6a. To localize fast bleaching sites, we subtracted the last image in the stack from the first one, while assuming that the rapid bleaching was finished by the time the last image was acquired [24]. The images obtained by subtraction (ΔF1 and ΔF2) in Figure 6b depict different fast bleaching regions, especially in the highlighted sites (green outline) for which photobleaching analysis was applied. The amplitude maps calculated for the fluorescence signals obtained in F1 and F2 emission ranges are shown in Figure 6c. In the case of the first filter (F1), the most pronounced fluorescence bleaching is observed in the regions close to the cell interior. In contrast, the pronounced fluorescence bleaching in the second emission range (F2) was observed in the regions around the cells. Also, the time constant (τ) maps for F1 and F2 spectral ranges differ significantly (Figure 6c). The τ-values in the F1 range are two times lower in average than that in F2 range, which indicates faster bleaching in the former spectral range. Heterogeneity maps in Figure 6c suggest that the τ-distribution is much broader in the F1 range, while the widths of distributions in both ranges are higher at the cell sites. These results differ from the bleach time constant and heterogeneity maps calculated for the autofluorescence of the control sample. The maps (presented in Supporting information, Figure S5) show homogenous distribution of τ- and *h*-values with slight variations due to complex morphology of the early biofilm phase. Time-integrated emission maps (TIE) in Figure 6c depict corrected intensities for various factors such as illumination shading, saturation and autofluorescence. The resulted map of pixels represents the total intensity emitted by the fluorophores.

Taking into account that the fluorescent signals acquired in the F1 and F2 ranges correspond to, respectively, the tryptophan fluorescence in non-polar and polar environments (Figure 1d), the results obtained by the bleaching kinetics analysis suggest possible sites of the nanoparticle accumulation. The fluorescence signal in the F1 range comes mostly from the nanoparticles that are situated in the cell membrane. The collected signal in the F2 range comes from the functionalized nanoparticles in polar environment and indicates the accumulation of the nanoparticles on the cells surfaces as well as water channels between cells [14,15]. The results obtained by ultrastructural analyses of *C. albicans*

exposed to silver nanoparticles [8,11] are in agreement with our observations, and support assignment of the F1 and F2 spectral ranges to cell interior and exterior, respectively. For example, Vazquez-Munoz et al [11] reported that the Ag NPs aggregate outside the examined *C. albicans* cells, while also confirming their presence in the interior of the cells.

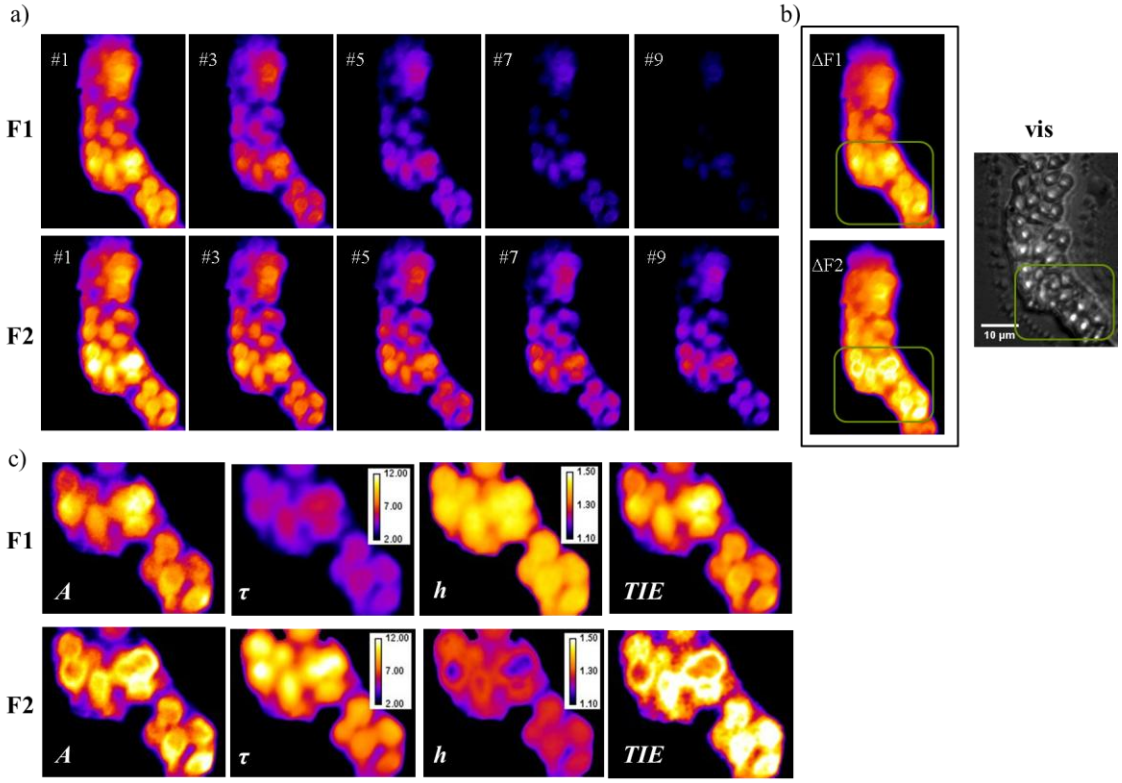

Figure 6. a) Five selected images of the AgTrp2.0 nanoparticles incubated cells obtained by time lapse imaging in [327 - 353 nm] (F1) and [370 – 410 nm] (F2) emission spectral ranges. b) The images (ΔF1 and ΔF2) obtained by subtraction of the last image in the stack from the first one in the specific spectral range and the VIS image of the cells. The analysis was carried out on the part of the image that depicted the most pronounced changes (green outline). c) Parameters from the stretch exponential fitting of the fluorescence intensity decay: A-amplitude map, τ-time constant map, h–heterogeneity map and TIE – Time integrated emission.

Conclusion

In this study, we used DUV fluorescence imaging to investigate the interaction of the tryptophan functionalized silver nanoparticles with polymorphic fungus *Candida albicans*. After the incubation with the functionalized nanoparticles, we tried to distinguish their fluorescence from the autofluorescence of the *C. albicans* polymorphs. Due to the environmentally sensitive fluorescence of the tryptophan on the surface of the nanoparticles, it was possible to investigate the origin of the fluorescence and search for the sites where the accumulation of the nanoparticles takes place. It was shown, without any doubt, that there is an increase in the fluorescence intensity upon incubation with the nanoparticles proving that they interacted with the cells. Two pseudohyphae with budding spores in early stage of growth were used to show that the interaction may depend on the polymorphic stage of the fungus. It was observed that the nanoparticles interacted with budding spores rather than with pseudohyphae filaments. The analyses of the fluorescence signals from the *C. albicans* cells showed that incubation results with an increase in the fluorescence intensity in both investigated spectral ranges ([327 - 353 nm] and [370 – 410 nm]). Therefore, by performing photobleaching tests, we were in position to identify the regions with the specific bleaching dynamics and associate them with the

polarity of the environment in which the nanoparticles are situated. Time integrated emission results obtained for the nanoparticle treated cells showed that the most pronounced fluorescence intensity was at the cell sites. This analysis suggested that the functionalized silver nanoparticles were predominantly situated at the surface of the *C. albicans* cells, but that they also penetrate the cell walls. These conclusions agree with the reported results obtained by ultrastructural analysis of the *C. albicans* cells incubated with silver nanoparticles.

Acknowledgments

Deep UV imaging of live fungi/fungus was performed at the DISCO beamline of Synchrotron SOLEIL (France) as a part of the research project N^{o} 20131218. We acknowledge with gratitude the TNA support granted by Synchrotron SOLEIL. The authors kindly acknowledge the help of Valerie Rouam (SOLEIL) for the help in the preparation of the samples for the fluorescence imaging. This study was financially supported by Ministry of Education and Science, Republic of Serbia (Project Nos. 172056, 45020 and 171020).

References

[1] I. D. Jacobsen, D. Wilson, B. Wächtler, S. Brunke, J. R. Naglik and B. Hube, Expert Rev. Anti Infect. Ther. 10 (2012) 85. doi: 10.1586/eri.11.152.

[2] A. Heintz-Buschart, H. Eickhoff, E. Hohn and U. Bilitewski, J. Biotechnol. 164 (2013) 137. doi: 10.1016/j.jbiotec.2012.12.004.

[3] S. Hawser, M. Francolini and K. Islam, J. Antimicrob. Chemother. 38 (1996) 579.

[4] Q. Yu, B. Zhang, F. Ma, C. Jia, C. Xiao, B. Zhang, L. Xing and M. Li, Chem. Biol. Interact. 227 (2015) 1. doi: 10.1016/j.cbi.2014.12.014.

[5] L. Ge, Q. Li, M. Wang, J. Ouyang, X. Li and M. M. Xing, Int. J. Nanomedicine 9 (2014) 2399. doi: 10.2147/IJN.S55015

[6] M. Rai, A. Yadav and A. Gade, Biotechnol. Adv. 27 (2009) 76. doi: 10.1016/j.biotechadv.2008.09.002.

[7] I. S. Hwang, J. H. Hwang, H. Choi, K. J. Kim and D. G. Lee, J Med Microbiol. 61 (2012) 1719. doi: 10.1099/jmm.0.047100-0.

[8] H. H. Lara, D. G. Romero-Urbina, C. Pierce, J. L. Lopez-Ribot, M. J. Arellano-Jiménez and M. Jose-Yacaman, J Nanobiotechnology 13 (2015) 91. doi: 10.1186/s12951-015-0147-8.

[9] K. Kim, W. Sung, B. Suh, S. Moon, J. Choi, J. Kim and D. Lee, Biometals 22 (2009) 235. doi: 10.1007/s10534-008-9159-2.

[10] I. S. Hwang, J. Lee, J. H. Hwang, K. J. Kim and D. G. Lee, FEBS J. 279 (2012) 1327. doi: 10.1111/j.1742-4658.2012.08527.x.

[11] R. Vazquez-Munoz, M. Avalos-Borja and E. Castro-Longoria, PLoS One 9 (2014) e108876. doi: 10.1371/journal.pone.0108876

[12] D. R. Monteiro, S. Silva, M. Negri, L. F. Gorup, E. R. de Camargo, R. Oliveira, D. B. Barbosa and M. Henriques, Mycoses 56 (2013) 672. doi: 10.1111/myc.12093.

[13] D. R. Monteiro, A. S. Takamiya, L. P. Feresin, L. F. Gorup, E. R. de Camargo, A. C. B. Delbem, M. Henriques and D. B. Barbosa, J Prosthodont Res 59 (2015) 42. doi: 10.1016/j.jpor.2014.07.004.

[14] D. R. Monteiro, L. F. Gorup, S. Silva, M. Negri, E. R. de Camargo, R. Oliveira, D. B. Barbosa and M. Henriques, Biofouling 7 (2011) 711. doi: 10.1080/08927014.2011.599101.

[15] D. R. Monteiro, S. Silva, M. Negri, L. F. Gorup, E. R. de Camargo, R. Oliveira, D. B. Barbosa and M. Henriques, J. Appl. Microbiol. 114 (2013) 1175. doi:10.1111/jam.12102

[16] A. Panacek, M. Kolar, R. Vecerova, R. Prucek, J. Soukupova, V. Krystof, P. Hamal, R. Zboril and L. Kvitek, Biomaterials 30 (2009) 6333. doi: 10.1016/j.biomaterials.2009.07.065.

[17] J. Chandra, D. M. Kuhn, P. K. Mukherjee, L. L. Hoyer, T. McCormick and M. A. Ghannoum, J. Bacteriol. 183 (2001) 5385. doi:10.1128/JB.183.18.5385-5394.2001.

[18] R. Dojcilovic, J. D. Pajovic, D. K. Bozanic, V. V. Vodnik, S. Dimitrijevic-Brankovic, A. R. Milosavljevic, S. Kascakova, M. Refregiers and V. Djokovic, Analyst 141 (2016) 1988. doi: 10.1039/c5an02358k.

[19] F. Jamme, S. Kaščaková, S. Villette, F. Allouche, S. Pallu, V. Rouam and M. Réfrégiers, Biol. Cell 105 (2013) 1. doi: 10.1111/boc.201200075.

[20] F. Jamme, S. Villette, A. Giuliani, V. Rouam, F. Wien, B. Lagarde and M. Réfrégiers, Microsc. Microanal. 16 (2010) 507. doi: 10.1017/S1431927610093852

[21] J. D. Pajović, R. Dojčilović, D. K. Božanić, S. Kaščáková, M. Réfrégiers, S. Dimitrijević-Branković, V. V. Vodnik, A. R. Milosavljević, E. Piscopiello, A. S. Luyt and V. Djoković, Colloids Surf B Biointerfaces 135 (2015) 742. doi: 10.1016/j.colsurfb.2015.08.050.

[22] A. Edelstein, N. Amodaj, K. Hoover, R. Vale, and N. Stuurman, Curr. Protoc. Mol. Biol. 14 (2012) 20.1

[23] J. Schindelin, I. Arganda-Carreras, E. Frise, V. Kaynig, M. Longair, T. Pietzsch, S. Preibisch, C. Rueden, S. Saalfeld, B. Schmid, J. Y. Tinevez, D. J. White, V. Hartenstein, K. Eliceiri, P. Tomancak and A. Cardona, Nat. Methods 9 (2012) 676.

[24] D. Wüstner, A. L. Larsen, N. J. Faergeman, J. R. Brewer and D. Sage, Traffic 11 (2010) 440. doi: 10.1111/j.1600-0854.2010.01040.x.

[25] M. N. Berberan-Santos, E. N. Bodunov and B. Valeur, Chem. Phys. 315 (2005) 171.

[26] K. C. Lee, J. Siegel, S. E. Webb, S. Leveque-Fort, M. J. Cole, R. Jones, K. Dowling, M. J. Lever and P. M. French, Biophys. J. 81 (2001) 1265.

[27] D. Wüstner, T. Christensen, L. M. Solanko and D. Sage, Molecules 19 (2014) 11096. doi: 10.3390/molecules190811096.

[28] R. I. MacCuspie,. J. Nanopart. Res. 13 (2011) 2893. doi: 10.1007/s11051-010-0178-x

[29] E. H. Smail, P. Briza, A. Panagos and L. Berenfeld, Infect. Immun. 63 (1995) 4078.

[30] P. M. Molyneux, S. Kilvington, M. J. Wakefield, J. I. Prydal and N. P. Bannister, Cornea 34 (2015) 1588. doi: 10.1097/ICO.0000000000000645.

[31] K. Y. Lum, S. T. Tay, C. F. Le, V. S. Lee, N. H. Sabri, R. D. Velayuthan, H. Hassan and S. D. Sekaran, Sci Rep 5 (2015) 9657. doi: 10.1038/srep09657.